24

BLOWN FILMS AND RIBBONS EXTRUSION

Jorge R. Robledo-Ortíz, Daniel E. Ramírez-Arreola,
Denis Rodrigue, and Rubén González-Núñez

24.1 INTRODUCTION

Sheet and bag manufacturing by blown film and ribbon extrusion represents a large segment of the plastics industry. A recent review on the situation and outlook of plastic films was presented by Pardo [1]. This chapter covers various aspects of polymer materials and/or their applications in specific end-products. In general, for most films, the main end-user is the packaging industry. A wide variety of plastic materials are used to produce films, essentially polyolefin, poly(ethylene terephthalate) (PET) for magnetic and optical applications, poly(vinyl chloride) (PVC) for consumer goods and medical applications, and poly(vinyl butyral) (PVB) for automobile applications [1]. An approach to improve film properties is to directly use blends of commercial polymers. These blends are generally easier to process, require lower investments, and do not require the development of new molecules for each specific application. The final film properties of such blends depend on the individual component properties, morphology, interphase, composition, and processing method [2]. The process consists of the following steps: extrusion of a polymer melt through a die, stretching, and cooling in air or water. In general, cooling occurs at a short distance from the die exit and the process is considered isothermal. Nevertheless, depending on the cooling distance, nonisothermal conditions can prevail. Blow extrusion and ribbon extrusion vary in the design of die used and in the type of cooling. The design and operation of the extruder up to the die is the same for both methods. The basic extrusion process is designed to continuously shape a thermoplastic material into a specific form.

This chapter includes, first, a general description of blown film and ribbon extrusion, including the most important parameters that need to be controlled. In section 24.3, the equations used to calculate the final dimensions of films and ribbons are presented. In that section, nonisothermal and non-Newtonian flow behavior is considered. A historical development of the different models available in the literature is also included. The relationship between the cooling process and the stretching forces is discussed in section 24.5. Section 24.6 deals with the relationships between morphology and mechanical properties for immiscible polymer blends.

24.2 EXTRUSION PROCESSES FOR BLOWN FILMS AND RIBBONS

The blown film process involves the extrusion of a polymer melt through an annular die and the subsequent blowing of the tube shaped. The materials used to produce films can be neat components, blends of two or more polymers, virgin materials, recycled materials, or blends of those. Additives such as slip, antiblock, antistatics, or pigments can also be added into the extruder feed.

The extrusion process is usually carried out in single- or twin-screw extruders. The molten polymer flows through an annular die in the following stage of the process. The flow through the die must be uniform across the exit plane; however, this gets complicated because of the nonlinear dependence of polymer viscosity on temperature and shear rate in the die. In this sense, a good die design is essential for optimal processing. The polymer tube is inflated by introducing air through a duct in the center of the die, maintaining a constant pressure. The bubble is pulled upward by means of a roller system at a specific rate to obtain the desired thickness and diameter.

Handbook of Polymer Synthesis, Characterization, and Processing, First Edition. Edited by Enrique Saldívar-Guerra and Eduardo Vivaldo-Lima.

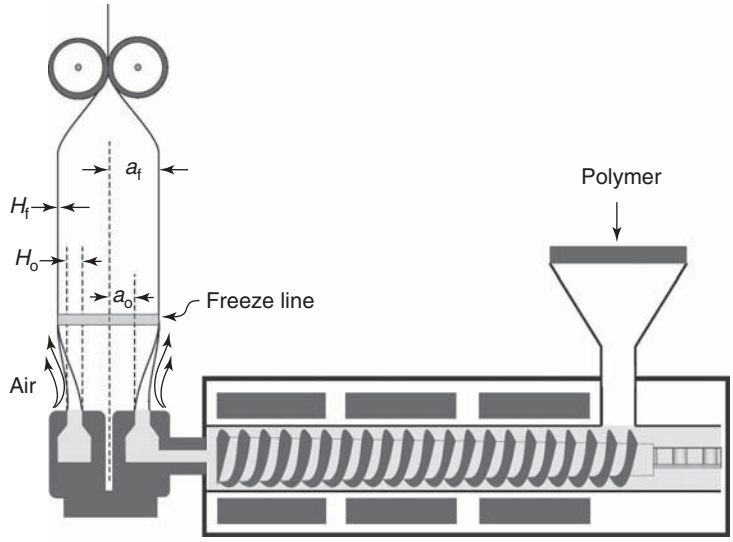

Figure 24.1 Schematic representation of the blown film process.

The cooling process is carried out through a ring placed on the die that provides air at high speed. Thickness and bubble diameter can also be controlled by changing, in addition to the take-up roller velocity, the cooling rate and pressure inside the bubble.

There are some characteristic parameters in the blown film process (see Fig. 24.1): the blow-up ratio (BUR), which is the ratio between the final radius (a_f) and the radius at the die exit (a_0); the thickness ratio (TR) calculated as the ratio of thickness at the die exit (H_0) and the final film thickness (H_f); and the draw ratio (DR) defined as the ratio of take-up roller velocity (V_f) to the extrusion velocity (V_0). The stretching force (F_z) is the force needed to take up the bubble by the roller system (Fig. 24.1).

A relationship among TR, DR, and BUR for stable bubble operation can be obtained from a mass conservation analysis as:

$$\frac{1}{\mathrm{TR}} = \frac{(a_0 + H_0)^2 - R_0^2}{2a_0 H_0}\left(\frac{\rho_m}{\rho_s}\right)\frac{1}{\mathrm{DR}\times\mathrm{BUR}} \qquad (24.1)$$

where ρ_m and ρ_s are the melt and solid polymer densities, respectively. This equation shows a linear relationship between TR^{-1} and $(\mathrm{DR}\cdot\mathrm{BUR})^{-1}$.

On the other hand, the ribbon extrusion process consists of the following steps: extrusion of a polymer melt through a small rectangular die, stretching, and cooling with air or water. Depending on the cooling distance, nonisothermal or isothermal conditions can be considered.

The ribbon extrusion process is studied using the following assumptions: steady state, incompressible flow, the velocity component in the stretching direction is the only function of this direction, each cross section remains rectangular, and temperature is assumed constant on a cross section.

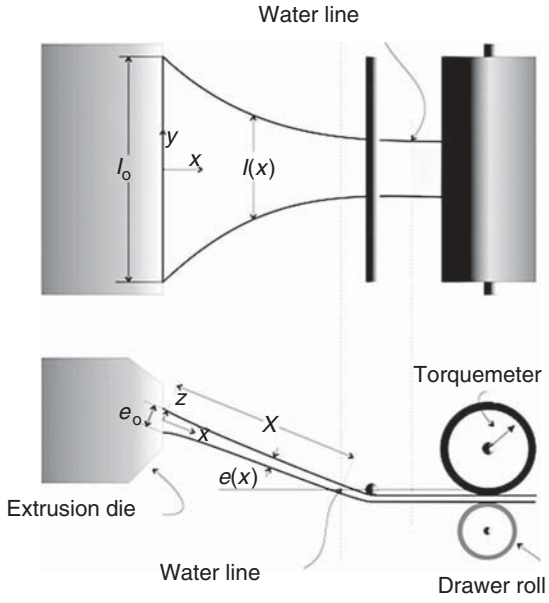

Figure 24.2 Schematic representation of the ribbon extrusion process.

There are also characteristic parameters of the process (see Fig. 24.2): distance in the stretching direction (x); total cooling length (X); cooling length in air (X_a); cooling length in water (X_w); ribbon width (l); die and initial ribbon widths (l_0); ribbon thickness (e); and die gap and initial ribbon thickness (e_0). DR is defined in the same way as in blown film processes and the stretching force (F) is the force needed to take off the ribbon by the roller system.

TABLE 24.1 Blown Film Modeling

Author(s)	Description
Pearson and Petrie [3, 4]	Newtonian model, isothermal
Han and Park [5, 6]	Power-law model, nonisothermal
Petrie [7]	Newtonian, nonisothermal, gravity effects included
Luo and Tanner [8]	Maxwell and Leonov models, nonisothermal
Kanai and White [9]	Newtonian model, nonisothermal including the effect of polymer crystallization
Cao and Campbell [10]	Nonisothermal Maxwell model extended past the freeze line with the Hookean elastic behavior
Sidiropoulos et al. [11]	Modified nonisothermal Newtonian model
Doufas and McHugh [12]	Model including flow-induced crystallization in the blown film
Muke et al. [13]	Nonisothermal, Kelvin viscoelastic model
Zatloukal and Vlcek [14, 15]	Variational principles to describe bubble shapes
Rao and Rajagopal [16]	Simulation for semicrystalline polymers
Robledo-Ortiz et al. [17]	Describes a correction factor to predict more precisely stretching force values
Shin et al. [18]	Multiplicity, bifurcation, stability, and hysteresis in dynamic solutions, nonisothermal viscoelastic model
Pirkle et al. [19]	Parameter estimation to characterize convective heat transfer
Pirkle and Braatz [20, 21]	Two-phase microstructural constitutive equation combined with the thin-shell model and dynamic model including the effect of crystallization
Housiadas [22]	Model including the aerodynamic effect of the air jet
Lee et al. [23]	Nonlinear dynamic behavior, nonisothermal film blowing with constant bubble pressure

24.3 EQUATIONS

24.3.1 Blown Film Equations

The blown film process has been studied analytically since the early 1970s (Table 24.1). The first analysis was proposed by Pearson and Petrie [3, 4], who followed a fluid mechanics approach. However, this model is restricted to Newtonian fluids under isothermal conditions. This first model has been modified several times to consider different aspects of the process, such as temperature variation and rheological behavior of the system.

The majority of the studies presented in Table 24.1 focus on the final dimensions of the blown films. However, the calculated stretching forces are not in close agreement with the reported experimental values.

It is possible to model the deformation of film bubbles with a system of dimensionless equations that is derived according to the following assumptions [13]: steady-state and axisymmetrical flow (z-axis) of an incompressible fluid; thin and flat film; external forces on the bubble are neglected; Newtonian, pseudoplastic, or viscoelastic fluids; and linear temperature profiles between die exit and freeze-line position. The system of dimensionless fundamental equations can be represented, irrespective of the rheological constitutive equation used, as shown in the following equations:

$$L = \frac{\left(A + Br^2\right)\left(1 + r'^2\right)^{1/2}}{r\,h} \tag{24.2}$$

$$r'' = \frac{\left[h\,C\,\left(1 + r'^2\right)^{1/2} - 2r\,B\,\left(1 + r'^2\right)\right]}{A + B\,r^2} \tag{24.3}$$

Each dimensionless quantity in these equations is defined as [3, 4]:

$$L = \frac{a_0\,\sigma_{11}}{V_0\,\eta_0} \tag{24.4a}$$

$$C = \frac{a_0\,\sigma_{33}}{V_0\,\eta_0} \tag{24.4b}$$

$$r = \frac{a}{a_0} \tag{24.4c}$$

$$h = \frac{H}{H_0} \tag{24.4d}$$

$$A = \frac{F_z\,a_0}{\eta_0\,Q} - B\,(\mathrm{BUR})^2 \tag{24.4e}$$

$$\mathrm{BUR} = \frac{a_f}{a_0} \tag{24.4f}$$

$$B = \frac{\pi\,a_0^3\,\Delta P}{\eta_0\,Q} \tag{24.4g}$$

where σ_{11} and σ_{33} are the main normal stresses, V_0 is initial velocity, a is radius, a_0 is initial radius, H is film thickness, H_0 is initial film thickness, F_z is stretching force, η_0 is Newtonian viscosity evaluated at T_0, Q is volumetric flow rate, ΔP is pressure difference, G_0 is elastic modulus, T_0 is extrusion temperature (die), and T is temperature.

For the Kelvin model, second-order and first-order equations for radius and thickness, respectively, are obtained. Rewriting the second-order equation as two first-order equations the system is transformed into the following equations [13]:

$$r_1' = r_2 \tag{24.5}$$

$$r_2' = \frac{1}{2r_1^2\left(A + Br_1^2\right)}\left[2\alpha r_1^2 h\left(1 + r_2^2\right)^{1/2}\ln(r) + 6\beta r_2 + r_1\left(1 + r_2^2\right)\left(A - 3Br_1^2\right)\right] \tag{24.6}$$

$$h' = h\left[-\frac{r_2}{2r_1} + \frac{\alpha}{4\beta}r_1 h\left(1 + r_2^2\right)\ln\left(\frac{1}{r_1^2 h^4}\right) - \frac{\left(A + Br_1^2\right)\left(1 + r_2^2\right)}{4\beta}\right] \tag{24.7}$$

where α is dimensionless shear modulus and β is dimensionless zero shear viscosity, defined as follows:

$$\alpha = \frac{a_0 G_0(T)}{v_0 \eta_0\left(T_0\right)} \tag{24.8a}$$

$$\beta = \frac{\eta_0(T)}{\eta_0\left(T_0\right)} \tag{24.8b}$$

For the Newtonian case, $\alpha = 0$, and for the pseudoplastic case,

$$\beta = \frac{\eta\left(T, \dot{\gamma}\right)}{\eta_0} \tag{24.9}$$

An extended mathematical development is presented by Muke et al. [13]. The dependence of viscosity on temperature is represented by an Arrhenius equation, as shown in the following equation:

$$\eta(T) = \eta\left(T_{\text{ref}}\right)\exp\left[\frac{E_a}{R}\left(\frac{1}{T} - \frac{1}{T_{\text{ref}}}\right)\right] \tag{24.10}$$

The rate of deformation is calculated as shown in the following equation:

$$\dot{\gamma} = \frac{Q}{2\pi\left(1 + r'^2\right)^{1/2} r h a_0^2 H_0}\left[\left(\frac{r'}{r}\right)^2 + \left(\frac{h'}{h}\right)^2 + \left(\frac{h'r'}{hr}\right)\right]^{1/2} \tag{24.11}$$

In the case of blown film simulations, a linear temperature profile can be used to obtain a greater stability in the solution of the system. The set of boundary conditions imposed on the system is given as shown in the following equation:

$$\text{for} \quad x = X, \quad \begin{Bmatrix} r_1 = \text{BUR} \\ r_2 = 0 \\ h = h_f \end{Bmatrix} \quad \text{and for} \quad x = 0, \quad \begin{Bmatrix} r_1 = 1 \\ h = h_0 \end{Bmatrix} \tag{24.12}$$

24.3.2 Ribbon Extrusion Equations

The physical and mathematical description of the ribbon extrusion process was first given by Pearson [24], who simplified the conservation equations by using a one-dimensional, isothermal, Newtonian fluid approach, and neglected the effects of polymer solidification. As in the case of blown film processes, several modifications and models have been proposed for the ribbon extrusion process (Table 24.2).

Considering the assumptions previously mentioned for the study of ribbon extrusion and the fact that the flow is mostly elongational, which means that the shear components are neglected, the velocity gradient ($\dot{\varepsilon}$) and the volumetric flow rate (Q) are given by the following equations:

$$[\dot{\varepsilon}] \approx \begin{bmatrix} \dfrac{\partial u}{\partial x} & 0 & 0 \\ 0 & \dfrac{\partial v}{\partial y} & 0 \\ 0 & 0 & \dfrac{\partial w}{\partial z} \end{bmatrix} \tag{24.13}$$

$$\frac{dQ}{dx} = \frac{d(u\,e\,l)}{dx} = 0 \tag{24.14}$$

For a Newtonian polymer, the stress tensor ($\boldsymbol{\tau}$) becomes

$$[\boldsymbol{\tau}] = 2\eta\,[\dot{\varepsilon}] - p\,[\mathrm{I}] \tag{24.15}$$

where p is the hydrostatic pressure, given by the following equation:

$$p = -\frac{1}{3}\left[\tau_{xx} + \tau_{yy} + \tau_{zz}\right] \tag{24.16}$$

TABLE 24.2 Ribbon Extrusion Modeling

Author(s)	Description
Pearson [24]	Newtonian model, isothermal
Cotto et al. [25]	The isothermal restriction was eliminated for biaxial deformation
Iyengar and Co [26]	Giesekus constitutive equation
Silagy et al. [27]	Viscoelasticity effects included
Acierno et al. [28]	Newtonian model, nonisothermal
Lamberti et al. [29]	Cross viscosity model including the effect of polymer crystallization
Satoh et al. [30]	Nonisothermal flow, viscoelastic fluid by the Larson model
Ramirez et al. [31]	Stretching force calculated using the nonisothermal Kelvin–Voigt model
Hallmark [32]	New method to measure polymer deformation during film casting
Lamberti [33]	Flow-induced crystallization

From the boundary conditions and neglecting the friction with air,

$$\mathbf{v} \cdot \mathbf{n} = 0 \tag{24.17}$$

$$[\tau] \cdot \mathbf{n} = 0 \tag{24.18}$$

The following set of equations results from the conservation of momentum for a Newtonian fluid [29]:

$$\frac{\mathrm{d}F}{\mathrm{d}x} = 0 \tag{24.19}$$

$$\frac{\mathrm{d}l}{\mathrm{d}x} = \frac{6\,Q\,\eta_0}{F\,l} - \sqrt{\left(\frac{6\,Q\,\eta_0}{F\,l}\right)^2 + 2} \tag{24.20}$$

$$\frac{\mathrm{d}u}{\mathrm{d}x} = \frac{u}{4}\left(\frac{F}{\eta_0\,Q} - \frac{2}{l}\frac{\mathrm{d}l}{\mathrm{d}x}\right) \tag{24.21}$$

$$\frac{\mathrm{d}e}{\mathrm{d}x} = -\frac{e}{u\,l}\left(u\frac{\mathrm{d}l}{\mathrm{d}x} - l\frac{\mathrm{d}u}{\mathrm{d}x}\right) \tag{24.22}$$

Neglecting viscous dissipation and assuming steady state, the conservation of energy can be written as [28, 29]

$$\frac{\mathrm{d}T}{\mathrm{d}x} = \frac{2\,h_\mathrm{c}\,l}{\rho\,C_\mathrm{p}\,Q}\left(T_\mathrm{a} - T\right) \tag{24.23}$$

where h_c is the convective heat transfer coefficient, C_p is the polymer heat capacity, and T_a is air temperature. Once the temperature profile is known, the change of viscosity with temperature is related to an Arrhenius expression (Eq. 24.10). To solve the set of ordinary differential Equations 24.17–24.23, the following boundary conditions are used:

$$\text{for} \quad x = 0, \quad \left\{\begin{matrix} e = e_0 \\ l = l_0 \\ u = u_0 \\ T = T_0 \end{matrix}\right\} \text{and}$$

$$\text{for} \quad x = X, \quad \left\{\begin{matrix} u = u_X \\ T = T_\mathrm{M} \equiv \text{Melt temperature} \end{matrix}\right\} \tag{24.24}$$

To eliminate the Newtonian simplification, a rheological constitutive equation is replaced in the equations that require it. Or, in the case where viscoelasticity effects are required, the simple Kelvin–Voigt model can be used. In this case, the stress is decomposed into its viscous and elastic components, as shown in the following equation:

$$\tau = G\,\varepsilon + \eta\,\dot{\varepsilon} \tag{24.25}$$

The Kelvin–Voigt model has the advantage of not needing the derivative of the stress, which is difficult to obtain experimentally, as in the Maxwell model.

24.4 RIBBON AND FILM DIMENSIONS

From numerical solution of the set of equations that represent both processes, it is possible to predict the ribbon and film dimensions and temperature profiles from the die to the freeze line. Figure 24.3 shows two-dimensional simulations of a PA6/LDPE blown film (extruded at 250 °C and DR = 20) and a PS/HDPE ribbon (extruded at 200 °C and DR = 4).

The numerical prediction of film and ribbon dimensions is strongly affected by the rheological model used. In general, in the case of blown film processes, good predictions of radius and curvature (angle) profiles can be obtained with any model because they mainly obey volume conservation. However, in several occasions not all the models give the same results for film thickness and stretching force. Figure 24.4 shows the predicted radius and angle profiles obtained from viscoelastic simulations, which are in agreement with experimental data for an LDPE blown film process. Similar predictions are obtained from Newtonian and pseudoplastic simulations. It is also observed that the bubble radius decreases and the freeze-line position increases with increasing values of DR.

As shown in Figure 24.5, similar results are observed for numerical simulations of ribbon dimensions (in dimensionless form). It is clear that all the rheological models tested (Newtonian, pseudoplastic, and viscoelastic) perform equally well in predicting thickness and width of the ribbon. As expected, once again the dimensions of the ribbon decrease with increasing DR.

24.5 COOLING PROCESS AND STRETCHING FORCE

The stretching force (F_z) highly affects the final dimensions, morphology, and stability of both processes. On the other hand, the position (from the die exit) at which molten polymer is solidified is defined as the freeze-line height (FLH) for the blown film process and as total cooling length for ribbon extrusion. The FLH can be controlled by the cooling process, increasing or decreasing the air velocity in film blowing or in the case of ribbon extrusion the cooling length is modified by increasing or decreasing the distance between the die exit and the cooling water bath.

The stretching force is a direct consequence of the distance of polymer solidification (DPS) in both processes (i.e., FLH in film blowing processes or cooling length in ribbon extrusion). In this sense, controlling DPS offers the possibility to control the final properties of films and ribbons. Table 24.3 lists typical values of stretching force as function of FLH and DR for blown films of LDPE.

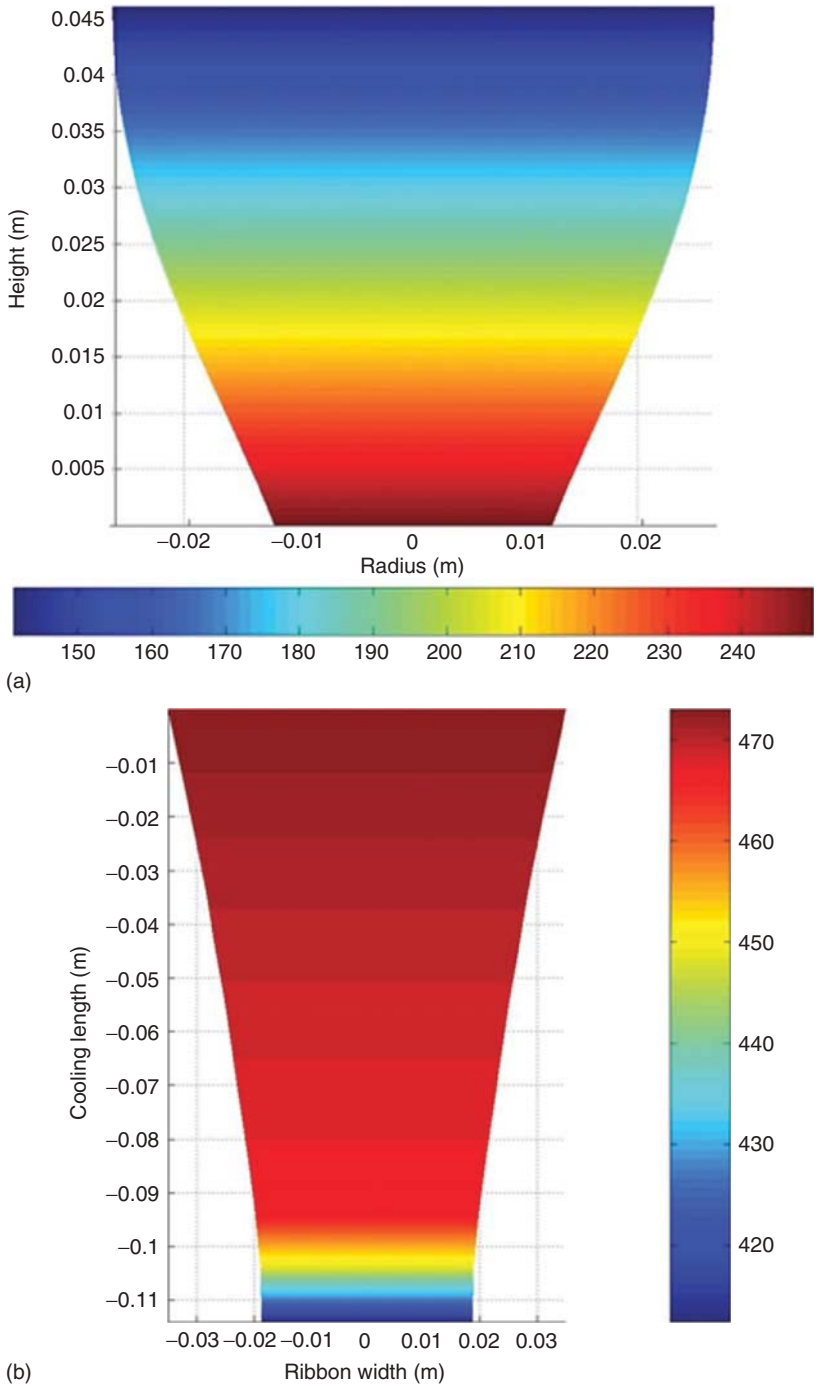

Figure 24.3 Simulated (a) bubble radius, (b) ribbon width, and temperature profiles. (*See insert for the color representation of the figure*.)

The stretching force and FLH increase with DR and, for a fixed DR, the stretching force decreases with increasing FLH.

In the same way, Figure 24.6 presents the stretching force (F) as a function of DR for different total cooling lengths (X). The stretching force increases with increasing DR, but decreases with increasing X. This behavior is attributed to the rheological properties of the polymer melt and a relaxation process for long water contact distances (in all the cases after a value of DR $\approx$ 6). There is also a maximum DR value that can be used before the ribbon breaks, which indicates limiting operation conditions.

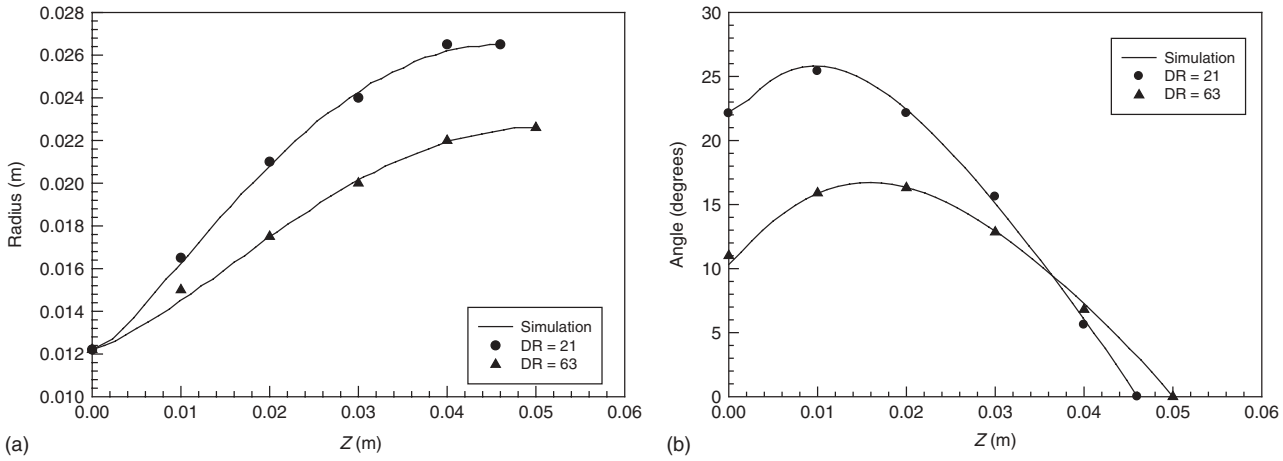

Figure 24.4 (a) Bubble radius and (b) curvature as function of DR.

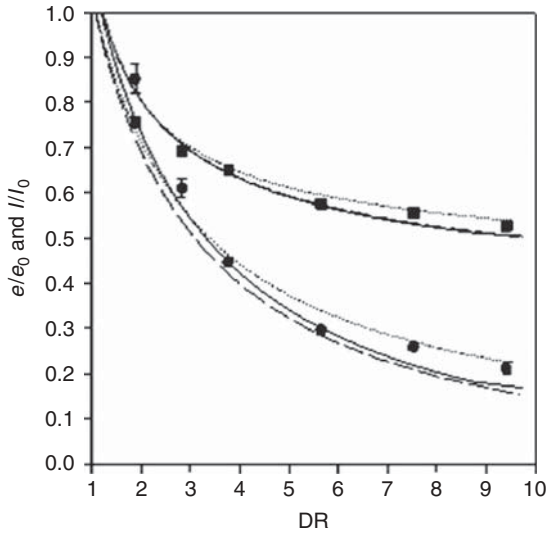

Figure 24.5 Dimensionless width (l/l_0) and thickness (e/e_0) of the ribbon as function of DR. Symbols are experimental data (●, thickness; ■, width) and lines are the predictions. Newtonian (·····), pseudoplastic (-----), and viscoelastic (—).

TABLE 24.3 Experimental Stretching Force (F_z) as Function of Freeze-Line Position (Z) and Draw Ratio (DR) for LDPE Films

DR = 14		DR = 21		DR = 27	
Z(m)	F(N)	Z(m)	F(N)	Z(m)	F(N)
0.046	1.388	0.052	1.452	0.058	1.516
0.052	1.310	0.055	1.390	0.059	1.460
0.056	1.220	0.057	1.310	0.060	1.390

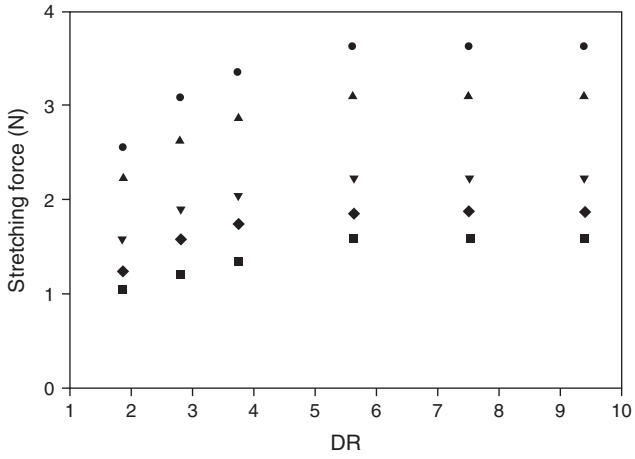

Figure 24.6 Experimental data for the stretching force (F) as function of DR under different water contact distances (X) values for HDPE ribbons: ●, 3.5 cm; ▲, 5 cm; ▼, 10 cm; ♦, 15 cm; and ■, 20 cm.

24.6 MORPHOLOGY AND MECHANICAL PROPERTIES

Several studies focused on the hot stretching postextrusion of polymer blends and their effect on mechanical properties to obtain specific final products characteristics have been reported [34–37]. The morphology of a dispersed phase in a matrix is strongly affected by the processing conditions and it is reflected on the final physical and mechanical properties. Figure 24.7 shows longitudinal micrographs of blown films obtained with a blend of 6% of PA6 with LDPE. It is clear that the deformation of the dispersed phase is greater when the position of the cooling line is lower, as the stretching force is greater when the position of the cooling line is lower. In the same way, the deformation increases with higher DR values. On the other hand, in the case of the transverse direction (TD), negligible changes in particle deformation are observed.

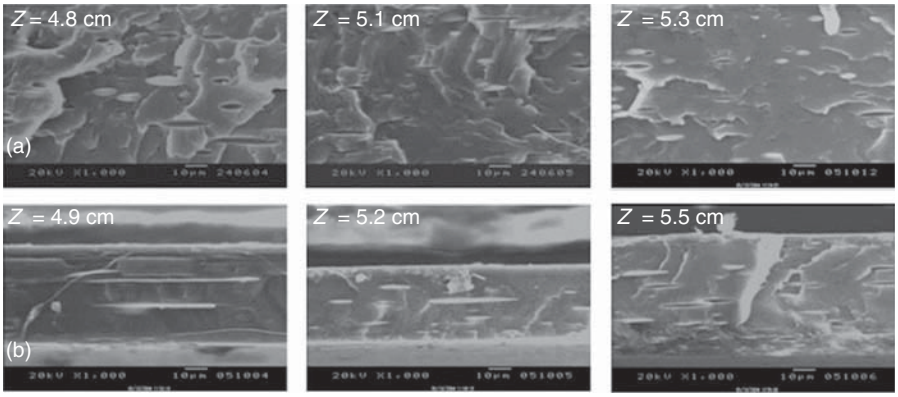

Figure 24.7 Longitudinal micrographs of 6% PA6–/LDPE films for (a) DR = 14 and (b) DR = 21 at different FLH.

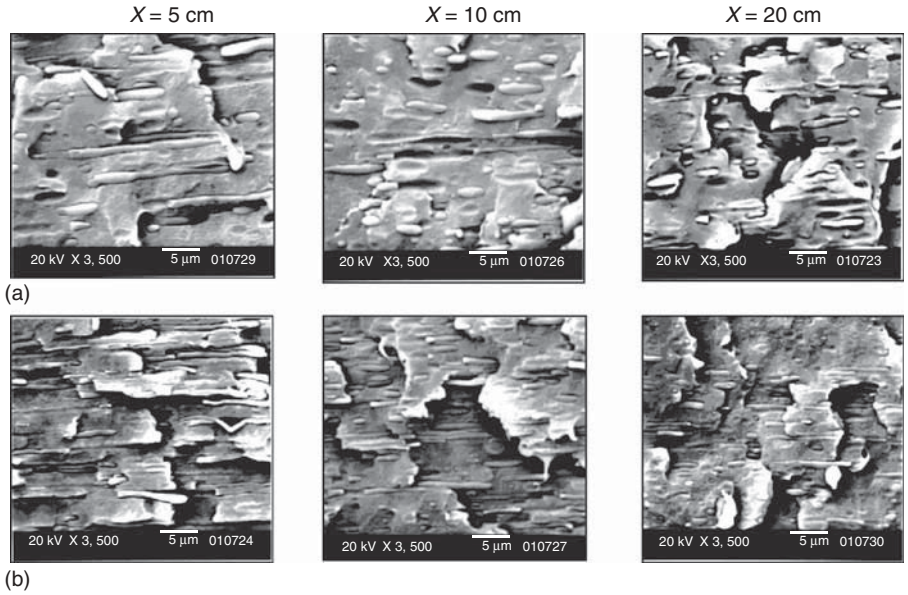

Figure 24.8 Micrographs of 9% PS/HDPE ribbons for (a) DR = 3.76 and (b) DR = 5.64.

Figure 24.8 shows SEM micrographs for ribbons of 9% PS in HDPE under different DR and X values. Similar to blown films, it is observed that deformation increases with increasing DR, but decreases with increasing X. This behavior is attributed to a larger stretching force, F, which increases with increasing DR and decreasing water contact distance. Similar behavior is observed for different contents of PS in HDPE.

It is well known that the mechanical properties of polymer blends strongly depend on the raw materials and on their final morphologies, which are controlled by interfacial adhesion, properties of the neat materials, and processing conditions, among others [2, 37–39].

Because of biaxial deformations in the blowing process, the tensile modulus is usually determined in both the machine direction (MD) and TD. Results obtained from tensile tests have been used to determine the tensile strength (nominal), elongation at break, and elastic modulus of the films. Table 24.4 lists the mechanical properties of LDPE and PA6/LDPE (with and without compatibilizer, Surlyn 9020, DuPont) films [40]. Mechanical properties are greatly affected by polymer molecular chain orientation [41].

For DR values between 10 and 50, a decrease in elastic modulus with DR is observed. In the case of a polymer blend, such as PA6/LDPE, there is an almost independent behavior of the tensile properties in the MD of noncompatibilized blends as a function of the dispersed phase concentration. However, in the TD, a clear dependence of the elastic modulus is observed. It is also observed that compatibilized films have higher modulus compared to noncompatibilized films. For the films presented in Table 24.4, PA6 particulate fibers

TABLE 24.4 Mechanical Properties of PA6/LDPE Films

		σ_p (MPa)		ε_b (%)		E (MPa)	
Film (%PA6)	DR	MD	TD	MD	TD	MD	TD
LDPE (0%)	18.4	11.5	7.7	298	166	133	122
	29.0	15.6	9.1	187	224	122	110
	50.5	31.9	20.1	151	300	107	96
10% Without Surlyn	19.9	21.7	6.1	410	99	174	162
	25.4	10.6	3.2	199	74	158	153
	32.3	7.1	2.7	127	36	156	126
30% Without Surlyn	12.6	22.0	8.4	504	11	187	146
	20.3	18.1	4.1	458	36	171	123
	36.2	22.8	—	469	—	137	—
10% With Surlyn	10.6	12.7	10.3	449	350	192	177
	25.5	15.1	9.3	359	210	185	164
	36.6	12.8	7.8	212	120	170	154
30% With Surlyn	12.3	15.7	7.0	365	48	238	194
	19.2	13.5	5.3	407	27	230	185
	34.5	12.4	6.7	258	24	224	168

Abbreviations: σ_p, tensile strength (nominal); ε_b, elongation at break; E, elastic modulus; MD, machine direction; TD, transverse direction; and DR, draw ratio.

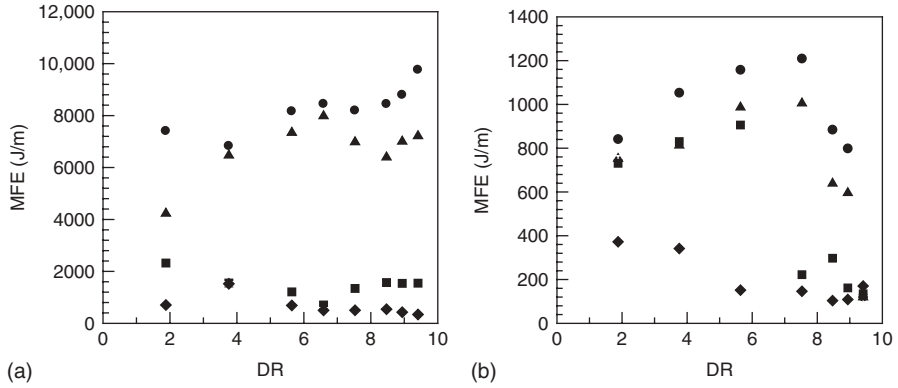

Figure 24.9 Mean failure energy for (a) 3% and (b) 9% PS in HDPE at different cooling lengths (X): ♦, 5 cm; ■, 10 cm; ▲, 15 cm; and ●, 20 cm.

(or lamellas) formed in the LDPE matrix during the deformation process are oriented in the flow direction (MD), which produces better mechanical properties than neat LDPE. This is also the reason properties in the TD are lower than in the MD.

Figure 24.9 shows the effect of cooling length (X) and DR on mean failure energy (MFE) for PS in HDPE. At low PS concentrations (3%), the variation of MFE with DR is relatively small but MFE varies substantially when the cooling length is changed. In the first case, the HDPE matrix sustains the impact energy mostly alone; whereas in the case where the cooling length increases, the relaxation process restraining further crystallization progresses. This makes the ribbons more stretchable, with better MFE properties. At low DR thicker samples are obtained. This facilitates the segregation of the crystalline part of the polymer on its amorphous part, creating failure points where fractures can propagate (low MFE values). Increasing DR, on the other hand, produces thinner ribbons and increased MFE values are observed due to greater MD orientation [42].

Another parameter influencing MFE is the blend morphology. By increasing DR, higher hydrodynamic stresses are transferred from the matrix to the dispersed phase, leading to increased deformation and MFE values. At low X values, the polymer is rapidly cooled down from the die exit and the particles do not have much time to relax because the morphology is frozen quickly. Depending on the concentration of the dispersed phase, a transition in the blend morphology from deformed spheroid and elongated particles to fiber formation is produced as DR increases. Particles may also coalesce. In general, it is observed that deformed particles increase MFE, whereas the formation of long fibers has the reverse effect. For high concentrations of the dispersed phase, increasing further DR decreases MFE,

which is attributed to fiber breakup. This behavior is observed in Figure 24.8 for DR = 5.64 and $X = 5$ cm. The corresponding MFE is presented in Figure 24.9.

REFERENCES

1. Pardo F. *Plastic Films; Situation and Outlook; A Rapra Market Report*. 1st ed. Shawbury: Rapra Technology Ltd; 2004. p 7.
2. Paul DR, Bucknall CB, editors. *Polymer Blends*. Volume 2. New York: Wiley; 2000. p 360.
3. Pearson JR, Petrie CJS. J Fluid Mech 1970;40:1.
4. Pearson JR, Petrie CJS. J Fluid Mech 1970;42:609.
5. Han CH, Park JY. J Appl Polym Sci 1975;19:3257.
6. Han CH, Park JY. J Appl Polym Sci 1975;19:3277.
7. Petrie CJS. AIChE J 1975;21:275.
8. Luo XL, Tanner RI. Polym Eng Sci 1985;25:620.
9. Kanai T, White JL. J Polym Eng 1985;5:135.
10. Cao B, Campbell GA. AIChE J 1990;36:420.
11. Sidiropoulos V, Tian JJ, Vlachopoulos J. J Plast Film Sheet 1996;12:107.
12. Doufas AK, McHugh AJ. J Rheol 2001;45:1085.
13. Muke S, Connell H, Sbarski I, Bhattacharya SN. J Non-Newt Fluid Mech 2003;116:113.
14. Zatloukal M, Vlcek J. J Non-Newt Fluid Mech 2004; 123:201.
15. Zatloukal M, Vlcek J. J Non-Newt Fluid Mech 2006;133:63.
16. Rao IJ, Rajagopal KR. Mech Adv Mater Struc 2005;12:129.
17. Robledo-Ortiz JR, Ramírez-Arreola D, González-Núñez R, Rodrigue D. J Plast Film Sheet 2006;22:287.
18. Shin DM, Lee JS, Jung HW, Hyun JC. J Rheol 2007;51:605.
19. Pirkle JC, Fujiwara M, Braatz RD. Ind Eng Chem Res 2010;49:8007.
20. Pirkle JC, Braatz RD. J Rheol 2010;54:471.
21. Pirkle JC, Braatz RD. J Process Contr 2011;21:405.
22. Housiadas KD. Polym Eng Sci 2011;51:1301.
23. Lee JS, Jung HW, Hyun JC. AIChE J 2011;57:3565.
24. Pearson JRA. *Mechanical Principles of Polymer Melt Processing*. 1st ed. New York: Pergamon Press; 1966. p 1.
25. Cotto D, Saillard P, Agassant JF, Haudin JM. *Interrelations Between Processing Structure and Properties of Polymeric Materials*. 1st ed. Amsterdam: Elsevier Science Ltd; 1984. p 1.
26. Iyengar VR, Co A. Chem Eng Sci 1996;51:1417.
27. Silagy D, Demay Y, Agassant JF. Polym Eng Sci 1996;36:2614.
28. Acierno D, Di Maio L, Ammirati CC. Polym Eng Sci 2000;40:108.
29. Lamberti G, Titomanlio G, Brucato V. Chem Eng Sci 2001;56:5749.
30. Satoh N, Tomiyama H, Kajiwara T. Polym Eng Sci 2001;41:1564.
31. Ramirez-Arreola D, Padilla-Lopez H, González-Núñez R, Rodrigue D. Int Polym Proc 2006;21:121.
32. Hallmark B. Polym Eng Sci 2008;48:37.
33. Lamberti G. Polym Eng Sci 2011;51:851.
34. Iñiguez CG, Michel E, González-Romero VM, González-Nuñez R. Polym Bull 2000;45:295.
35. Li ZM, Yang MB, Xe BH, Feng JM, Huang RW. Polym Eng Sci 2003;43:615.
36. Quan H, Zhong GJ, Li ZM, Yang MB, Xie BH, Yang SY. Polym Eng Sci 2003;45:1303.
37. Fasce L, Seltzer R, Frontini P, Rodriguez-Pita VJ, Pacheco EBAV, Dias ML. Polym Eng Sci 2005;45:354.
38. Huang HX, Huang YF, Li XJ. Polym Test 2007;26:770.
39. Dhoble A, Kulshreshtha B, Ramaswami S, Zumbrunnen DA. Polymer 2005;46:2244.
40. Lopez-Barron CR, Robledo-Ortiz JR, Rodrigue D, Gonzalez-Nuñez R. J Plast Film Sheet 2007:23,149.
41. Patel RM, Butler TI, Walton KL, Knight GW. Polym Eng Sci 1994;34:1506.
42. Ramírez-Arreola DE, Robledo-Ortíz JR, Moscoso F, González-Núñez R, Rodrigue D. Polym Eng Sci 2008;48:1600.